

## Electronic Supplementary Information

### Tuning the electronic structure of Co@N-C hybrids via metal-doping for efficient electrocatalytic hydrogen evolution reaction

Peiyun Zhou,<sup>a</sup> Linmeng Wang,<sup>a</sup> Junjun Lv,<sup>a</sup> Rushuo Li,<sup>a</sup> Fengyu Gao,<sup>b</sup> Xiubing Huang,<sup>a,\*</sup> Yunfeng Lu,<sup>c,\*</sup> and Ge Wang<sup>a,d\*</sup>

<sup>a</sup> Beijing Advanced Innovation Center for Materials Genome Engineering, Beijing Key Laboratory of Function Materials for Molecule & Structure Construction, School of Materials Science and Engineering, University of Science and Technology Beijing, Beijing 100083, P. R. China.

<sup>b</sup> School of Energy and Environmental Engineering, University of Science and Technology Beijing, Beijing 100083, P. R. China.

<sup>c</sup> Department of Chemical and Biomolecular Engineering, University of California, Los Angeles, California 90095, United States.

<sup>d</sup> Shunde Graduate School, University of Science and Technology Beijing, Shunde 528399, P. R. China.

**Corresponding authors:** Xiubing Huang, E-mail: xiubinghuang@ustb.edu.cn; Yunfeng Lu, E-mail: luucla@ucla.edu; Ge Wang, E-mail: gewang@ustb.edu.cn

## Experimental Details

**Chemicals:** Nickel foam (NF) was purchased from Shanghai Hesen Electric Corporation. Cobalt nitrate hexahydrate ( $\text{Co}(\text{NO}_3)_2 \cdot 6\text{H}_2\text{O}$ ) was purchased from Energy Chemical Corporation. Commercial Pt/C (20%), 2-methylimidazole (2-MI) and Nafion solution were purchased from Aladdin Chemical Reagent Corporation. Phosphotungstic acid hydrate ( $\text{H}_3\text{PW}_{12}\text{O}_{40} \cdot x\text{H}_2\text{O}$ ), ammonium fluoride ( $\text{NH}_4\text{F}$ ) and urea ( $\text{CO}(\text{NH}_2)_2$ ) were purchased from Innochem Corporation.

### *Sample preparation:*

*Preparation of CoW-hy@NF:* All nickel foams (2 cm × 4 cm) were carefully washed with acetone, hydrochloric acid (3 M) and deionized water for 30 minutes under ultrasonic conditions, respectively, to remove oil and oxides on the surface. Co1.5W0.5-hy@NF was synthesized through a typical hydrothermal procedure, where "1.5" and "0.5" represent the amount of Co and W added (mmol). Firstly,  $\text{Co}(\text{NO}_3)_2 \cdot 6\text{H}_2\text{O}$  (1.5 mmol, 437 mg),  $\text{H}_3\text{PW}_{12}\text{O}_{40} \cdot x\text{H}_2\text{O}$  (0.042 mmol, 120 mg),  $\text{CO}(\text{NH}_2)_2$  (10 mmol, 600 mg) and  $\text{NH}_4\text{F}$  (8 mmol, 296 mg) were taken into 36 mL ultra-pure water under magnetic stirring until a homogeneous solution was formed. Next, the solution was poured into a 50 mL Teflon-lined stainless-steel autoclave, and the pretreated NF was placed vertically into the autoclave. The sealed autoclave was kept at 120 °C for 10 hours, and after cooling to room temperature, the NF was taken out and washed 3 times with ultrapure water and absolute ethanol respectively, while the powder sample in the autoclave was collected by centrifugation. Finally, the as-synthesized sample was vacuum-dried at 60 °C overnight to get Co1.5W0.5-hy@NF. Similarly, Co2W0-hy@NF, Co1.75W0.25-hy@NF and Co1.25W0.75-hy@NF were prepared through the same approach except for the different molar ratios of Co source to W source.

*Preparation of CoW-mof@NF:* Co1.5W0.5-mof@NF was derived from Co1.5W0.5-hy@NF through a simple impregnation method. In detail, the Co1.5W0.5-hy@NF was added into a solution of 2-MI (1 M) and kept at 50 °C for 24 hours, then carefully washed several times with ethanol, followed by drying overnight in a vacuum drying oven at 60 °C, and finally the Co1.5W0.5-mof@NF was obtained. Similarly, Co2W0-mof@NF, Co1.75W0.25-mof@NF

and Co<sub>1.25</sub>W<sub>0.75</sub>-mof@NF were prepared.

*Preparation of CoW-py-T@NF:* Co<sub>1.5</sub>W<sub>0.5</sub>-py-500@NF was derived from Co<sub>1.5</sub>W<sub>0.5</sub>-mof@NF by a simple one-step pyrolysis under constant N<sub>2</sub> flow. In detail, the Co<sub>1.5</sub>W<sub>0.5</sub>-mof@NF was placed into a furnace tube, heated from 30 °C to 500 °C at a heating rate of two degrees Celsius per minute, and then kept at 500 °C for two hours, and finally the Co<sub>1.5</sub>W<sub>0.5</sub>-py-500@NF was obtained. The load mass density of Co<sub>1.5</sub>W<sub>0.5</sub>-py-500@NF is about 1 mg cm<sup>-2</sup>. Similarly, Co<sub>2</sub>W<sub>0</sub>-py-500@NF, Co<sub>1.75</sub>W<sub>0.25</sub>-py-500@NF and Co<sub>1.25</sub>W<sub>0.75</sub>-py-500@NF were prepared by the same pyrolysis procedure, except that the corresponding CoW-mof@NF precursors were used. Besides, Co<sub>1.5</sub>W<sub>0.5</sub>-py-400@NF and Co<sub>1.5</sub>W<sub>0.5</sub>-py-600@NF were prepared by the same pyrolysis procedure, except that the holding temperature was set to 400 °C and 600 °C, respectively.

*Preparation of Pt/C@NF:* Commercial Pt/C (10 mg) was well mixed with 900 μL ethanol and 100 μL 5% Nafion to create a homogeneous ink. Subsequently, 50 μL of the ink was evenly casted onto a piece of NF (0.5 cm × 1 cm) and dried at room temperature to obtain Pt/C@NF.

**Materials Characterization:** The microstructure and micromorphology were characterized by transmission electron microscopy (TEM, JEOL JEM-2010) and field emission scanning electron microscopy (FE-SEM, Hitachi SU8010). The crystal structures were identified by X-ray diffractometer (XRD, Bruker D8 Advance diffractometer, Cu K $\alpha$ 1,  $\lambda = 1.5406 \text{ \AA}$ ) measuring from 5 to 80 degrees (2-Theta) at a sweep rate of five degrees per minute. All XRD data were obtained by testing powder samples. The element distribution and content were acquired by FE-SEM/energy dispersive X-ray spectroscopy (FE-SEM/EDX, Hitachi SU8010/IXRF Systems) and inductively coupled plasma optical emission spectroscopy (ICP-OES, Agilent ICPOES 730). The chemical states of surface elements were detected by X-ray photoelectron spectroscopy (XPS, Thermo ESCALAB 250Xi), and the binding energy of C 1s peak (284.8 eV) was used as a reference value for correcting all binding energies. Raman spectrum was measured with a Renishaw inVia spectrometer under a laser with a wavelength of 532 nm. Thermogravimetric analysis (TGA, NETZSCH STA449F3, N<sub>2</sub> flow) was performed at a rate of ten degrees Celsius per minute from 40 to 800 °C to investigate the thermal decomposition behavior of as-obtained samples. Fourier transform infrared spectroscopy (FT-IR, Nicolet 6700,

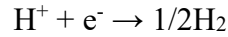
KBr particle technology) was performed in the region of 4000 to 500  $\text{cm}^{-1}$  to characterize the functional groups of as-obtained samples.

**Electrochemical Measurements:** A CHI 660D electrochemical workstation was used for all electrochemical measurements, and 1.0 M KOH (pH = 14) solution was used as electrolyte. The HER test was performed using a three-electrode system, in which the nickel foam supporting with the synthetic active species was directly employed as the working electrode, and the Hg/HgO electrode and graphite rod were used as the reference and auxiliary electrodes, respectively. Electrochemical impedance spectroscopy (EIS) measurements were performed at -1.1 V (vs. Hg/HgO) in the frequency range of 100 kHz to 0.01 Hz. All measured potentials were converted to potentials relative to reversible hydrogen electrode (RHE) through a formula:  $E(\text{vs. RHE}) = E(\text{vs. Hg/HgO}) + 0.098 + 0.0591 \times \text{pH}$ ; then the potentials were iR-compensated by another formula:  $E_{\text{compensated}} = E_{\text{measured}} - iR_s$  ( $R_s$ : the resistance of electrolyte solution, which is derived from the corresponding EIS result), while all stability tests were not iR-compensated. After cyclic voltammetry (CV) activation, linear sweep voltammetry curves (LSV) were recorded at a rate of two millivolts per second. Tafel slopes were calculated from the strong polarization regions of the corresponding polarization curves. Double-layer capacitance ( $C_{dl}$ ) values were determined by carrying out CV tests in the non-Faradaic regions at different scan rates (10, 20, 30, 40, 50, and 60  $\text{mV s}^{-1}$ ). Stability tests were performed by chronoamperometry measurements for 35 hours at a given potential. Faraday efficiency (FE) were recorded by the water drainage method.<sup>1</sup>

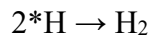
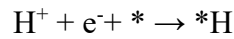
**DFT Calculations:** All calculations were performed by utilizing the spin-polarized density functional theory (DFT) via the CASTEP module imbedded in Material Studio.<sup>2</sup> The generalized gradient approximation (GGA) in the form of Perdew-Burke-Ernzerhof (PBE) functional were used to depict the electronic exchange and correlation effects.<sup>3,4</sup> The energy cutoff of plane-wave basis set was set to 500 eV, and the core electrons were handled with the OTFG ultrasoft pseudopotential. The self-consistent field (SCF) tolerance was set to  $1 \times 10^{-6}$  eV.<sup>5</sup> The Brillouin zone of the models were sampled at a  $(3 \times 3 \times 1)$  mesh. The Co@N-C heterostructure was modelled by a layer thickness of graphite and four layers thickness of Co

with their (001), (111) surface exposed, and then the slab model expanded to supercell including  $4 \times 4$  unit cells with the 15 Å thickness vacuum space.<sup>5</sup> The in-plane lattice of graphene was fitted that of Co with the lattice mismatch of 0.2% by the slightly compression. Then, N atoms were substituted into the graphene sheet, resulting in doping concentration of 12.5 at.%, approximate to the experimental value (13.8 at.%). For CoW@N-C heterostructure, W atoms were uniformly doped in Co@N-C heterostructure model with 6.3 at.% concentration which close to the experimental result (9.1 at.%). Tkatchenko-Scheffler (TS) scheme of dispersion correction was applied to describe the van der Waals (vdW) interactions in layered materials.<sup>6</sup> With fixed cell parameters and the bottom layer of metal atoms, the model structures were fully optimized using the convergence criteria of  $10^{-5}$  eV for the electronic energy,  $10^{-2}$  eV/Å for the forces and  $10^{-3}$  Å for the maximum displacement on each atom. It's worth noting that the C/N atoms in graphene layer are coordinated with metallic Co and W in above optimized structures, which is consistent with the XPS results.

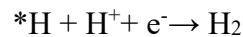
According to Nørskov's study, the computational hydrogen electron (CHE) model was utilized for calculating the Gibbs free energy in the HER process. The total hydrogen evolution reaction can be written as the following:<sup>7</sup>



An intermediate state in the above process takes place at an electrode supplying the electrons, describing as the below:



where the \* means the active site and \*H denotes a hydrogen atom adsorbed on the active site. The final hydrogen evolution step may also be the following:



For all the simulated models, the Gibbs free energy of the reaction is expressed by  $\Delta G_{\text{H}^*} = \Delta E_{\text{H}^*} + \Delta E_{\text{ZPE}} - T\Delta S + \Delta G_{\text{pH}} + \Delta G_{\text{U}}$ .  $\Delta G_{\text{pH}}$  means the free energy ascribing to  $\text{H}^+$  concentration. The  $\Delta G_{\text{pH}}$  is defined as  $\Delta G_{\text{pH}} = 2.303 \times k_{\text{B}}T \times \text{pH}$ , in which  $k_{\text{B}}$  is the Boltzmann constant ( $1.38 \times 10^{-23}$  J/K). The free energy attributed by electrode potential,  $\Delta G_{\text{U}}$ , is expressed as  $\Delta G_{\text{U}} = -n_{\text{e}}U$ , in which  $n_{\text{e}}$  denotes the number of electrons transferring to intermediates at HER steps and  $U$  represents the electrode potential. As for this work, the value of pH and  $U$  were set as zero to

simulate the above models. Therefore, the Gibbs free-energy ( $\Delta G_{H^*}$ ) can be calculated as  $\Delta G_{H^*} = \Delta E_{H^*} + \Delta E_{ZPE} - T\Delta S$ , where  $\Delta E_{H^*}$  is the adsorption energy of atomic hydrogen on the given models, defined by  $\Delta E_{H^*} = E(H^*) - E(^*) - 1/2E(H_2)$ . Moreover,  $\Delta E_{ZPE}$  and  $\Delta S$  denote zero-point energy and entropy change caused by H adsorption at 298.15 K, respectively. As the entropy of hydrogen in adsorbed state is negligible,  $\Delta S$  can be calculated as  $-1/2 S_0$  ( $S_0$  is the entropy of  $H_2$  at standard conditions). Hence, the free energy of the adsorbed state can be estimated based on literatures<sup>7-9</sup> as the following:

$$\Delta G_{H^*} = \Delta E_{H^*} + 0.24 \text{ eV}$$

## Results and Discussion

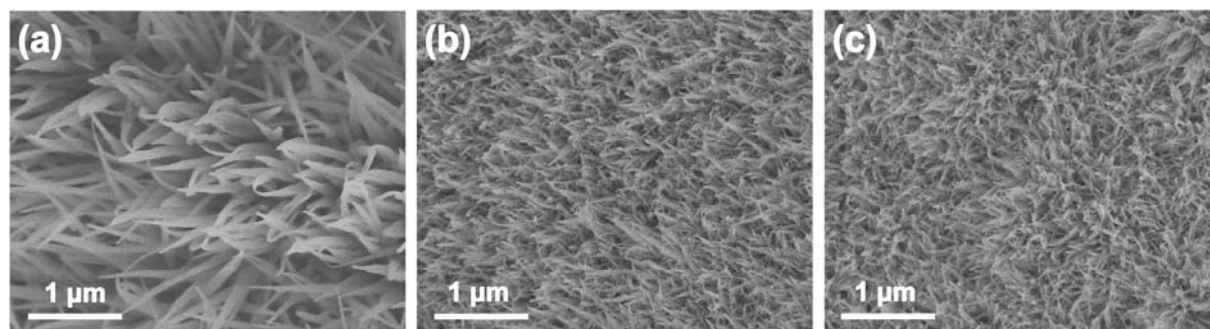


**Fig. S1.** SEM images of (a) Co<sub>2</sub>W<sub>0</sub>-hy@NF, (b) Co<sub>1.75</sub>W<sub>0.25</sub>-hy@NF and (c) Co<sub>1.25</sub>W<sub>0.75</sub>-hy@NF.

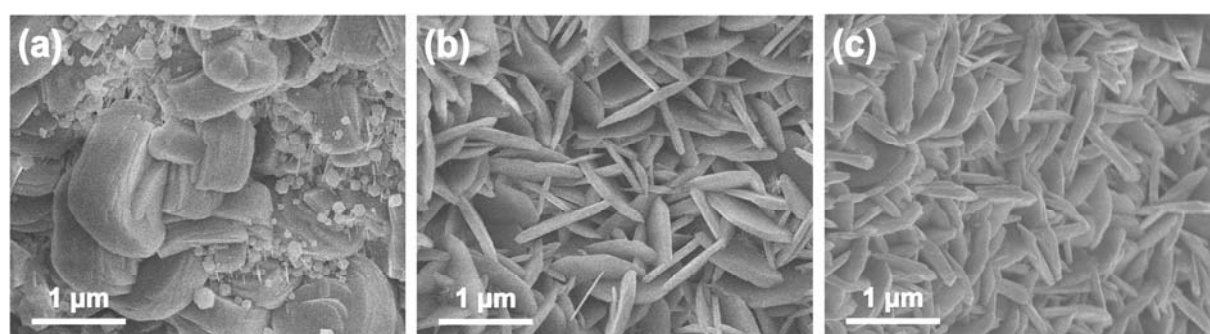


**Fig. S2.** SEM images of (a) Co<sub>2</sub>W<sub>0</sub>-mof@NF, (b) Co<sub>1.75</sub>W<sub>0.25</sub>-mof@NF and (c) Co<sub>1.25</sub>W<sub>0.75</sub>-mof@NF.

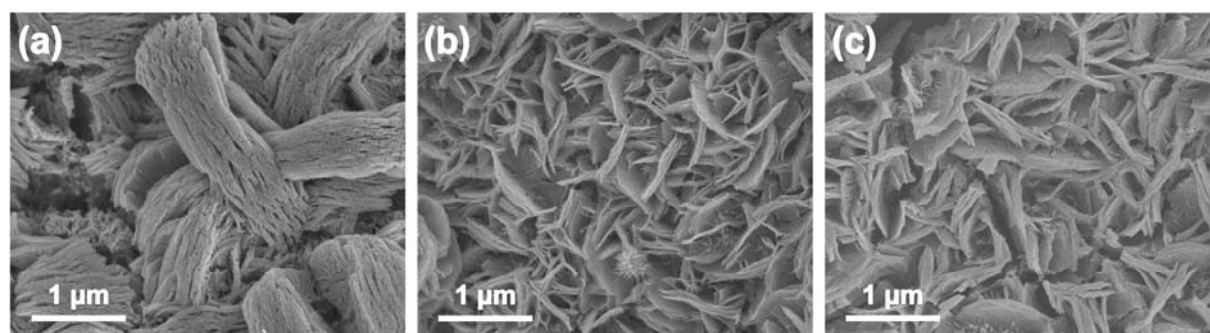


**Fig. S3.** SEM images of (a) Co<sub>2</sub>W<sub>0</sub>-py-500@NF, (b) Co<sub>1.75</sub>W<sub>0.25</sub>-py-500@NF and (c) Co<sub>1.25</sub>W<sub>0.75</sub>-py-500@NF.

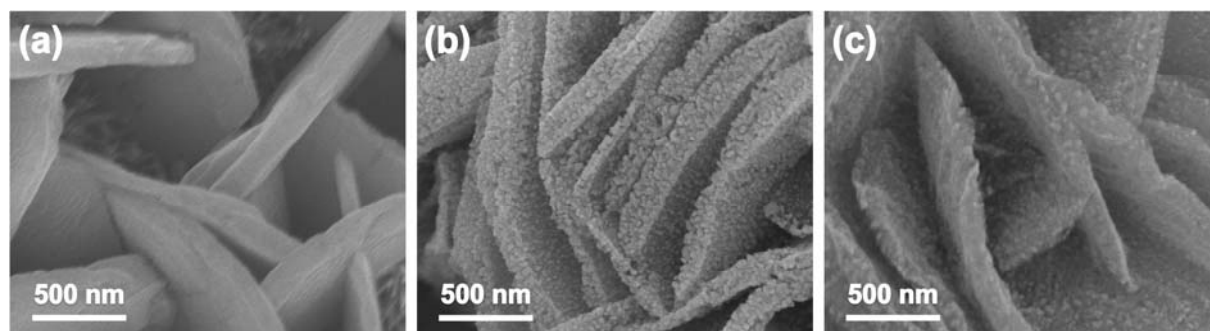


**Fig. S4.** SEM images of (a) Co<sub>1.5</sub>W<sub>0.5</sub>-py-400@NF, (b) Co<sub>1.5</sub>W<sub>0.5</sub>-py-500@NF and (c) Co<sub>1.5</sub>W<sub>0.5</sub>-py-600@NF.

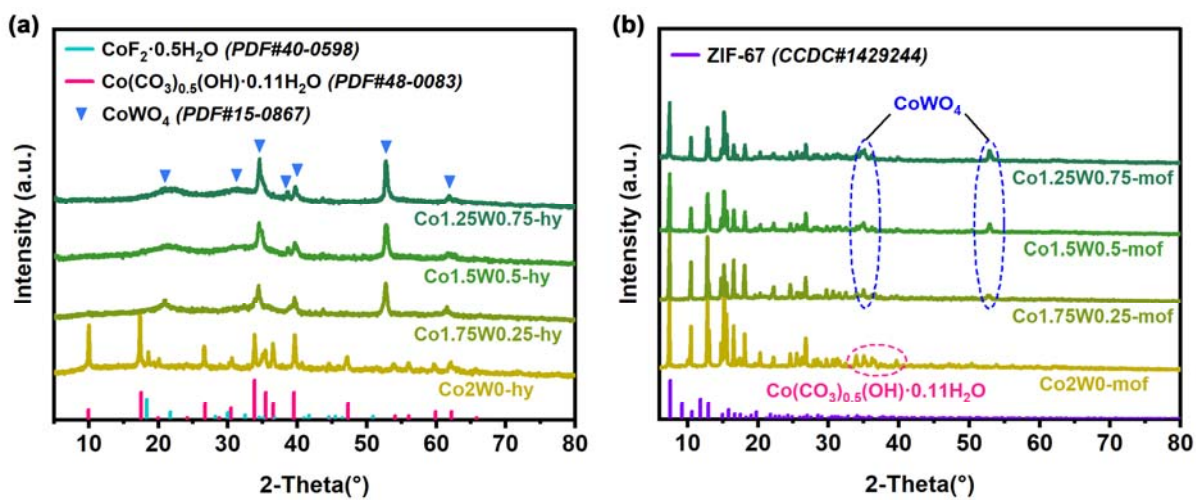


Fig. S5. XRD patterns of (a) CoW-hy and (b) CoW-mof.

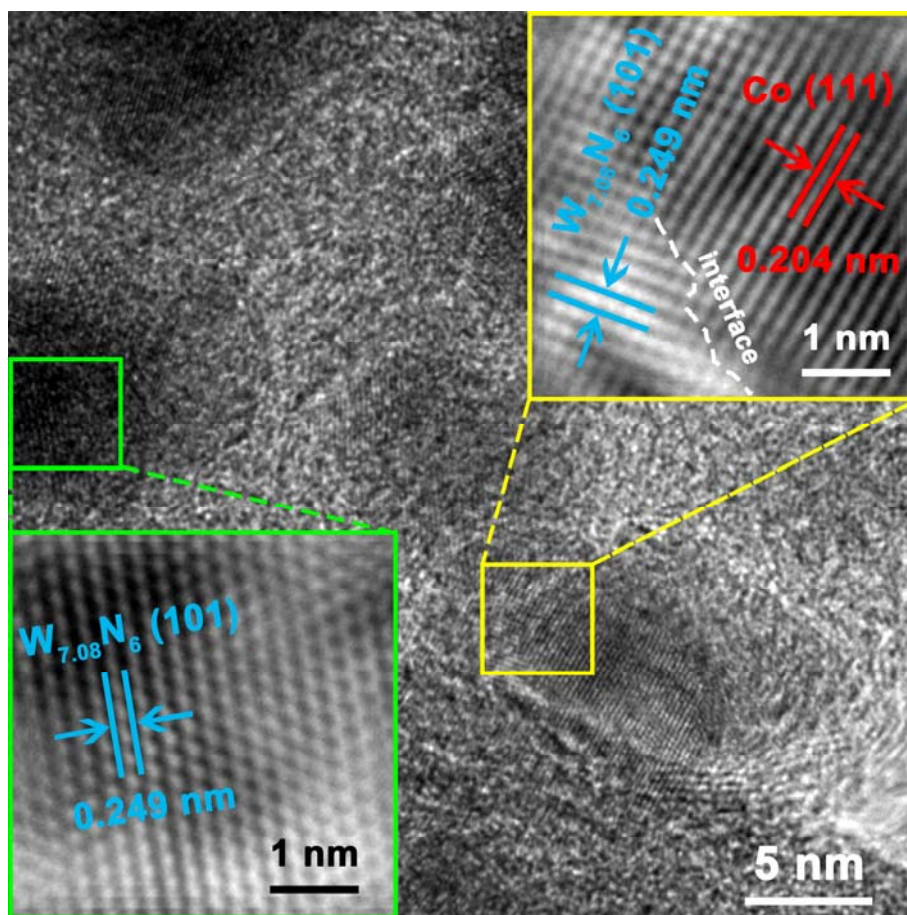


Fig. S6. HRTEM image of  $\text{Co}_{1.25}\text{W}_{0.75}\text{-py-500}$ .

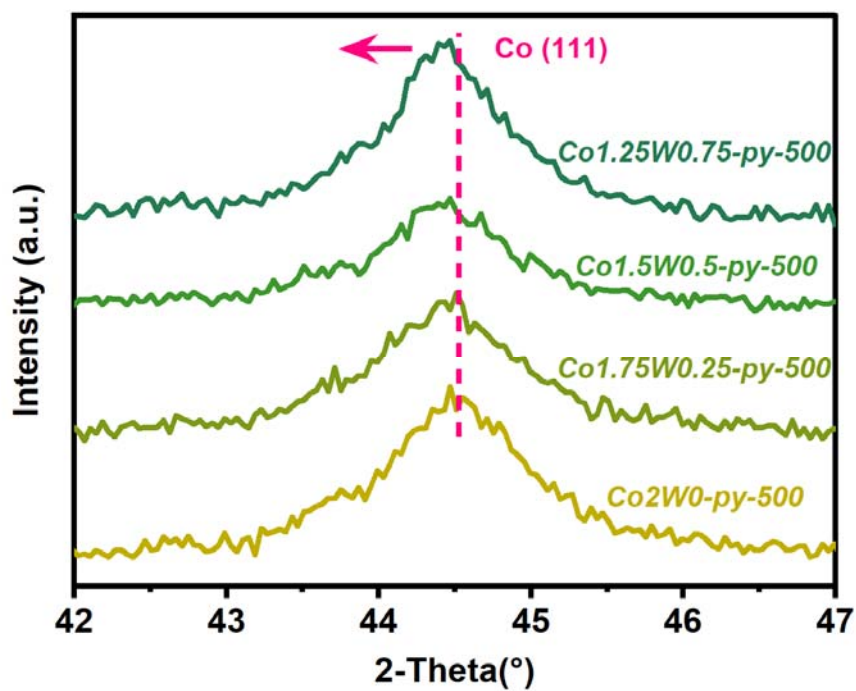


Fig. S7. The enlarged XRD patterns.

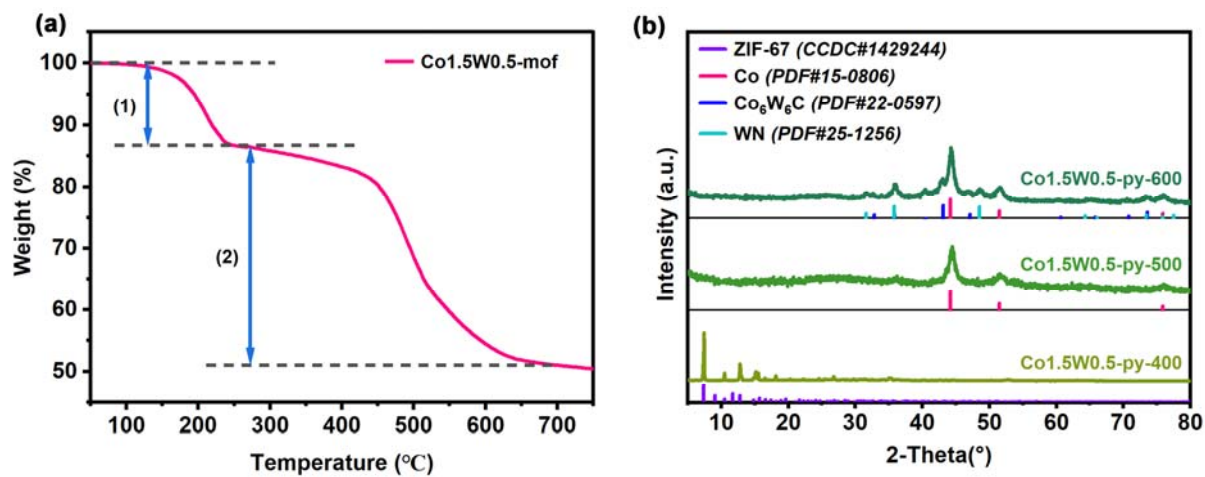


Fig. S8. (a) TGA curve of Co1.5W0.5-mof. (b) XRD patterns of CoW-py-T.

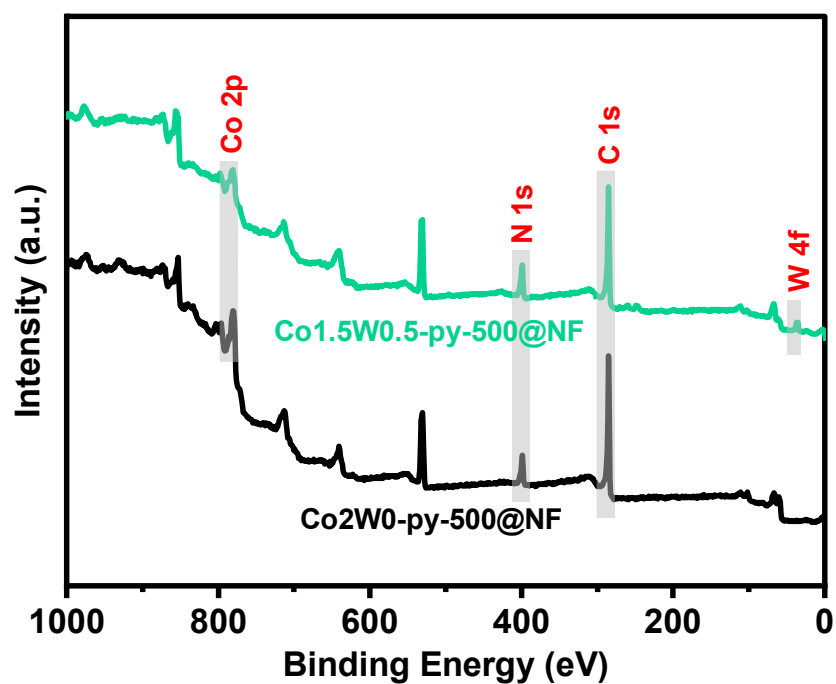


Fig. S9. XPS survey spectra of Co<sub>2</sub>W<sub>0.5</sub>-py-500@NF and Co<sub>1.5</sub>W<sub>0.5</sub>-py-500@NF.

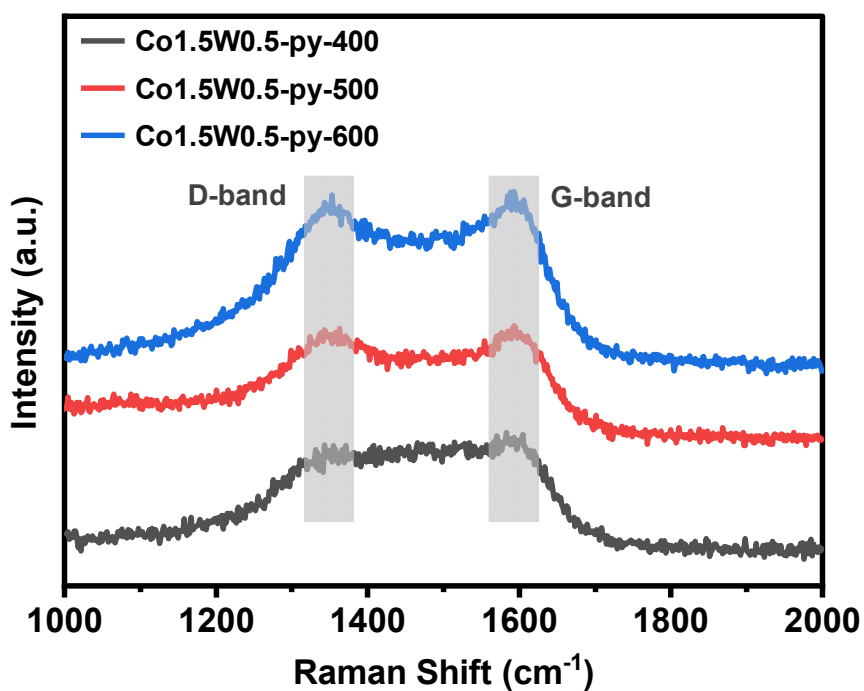
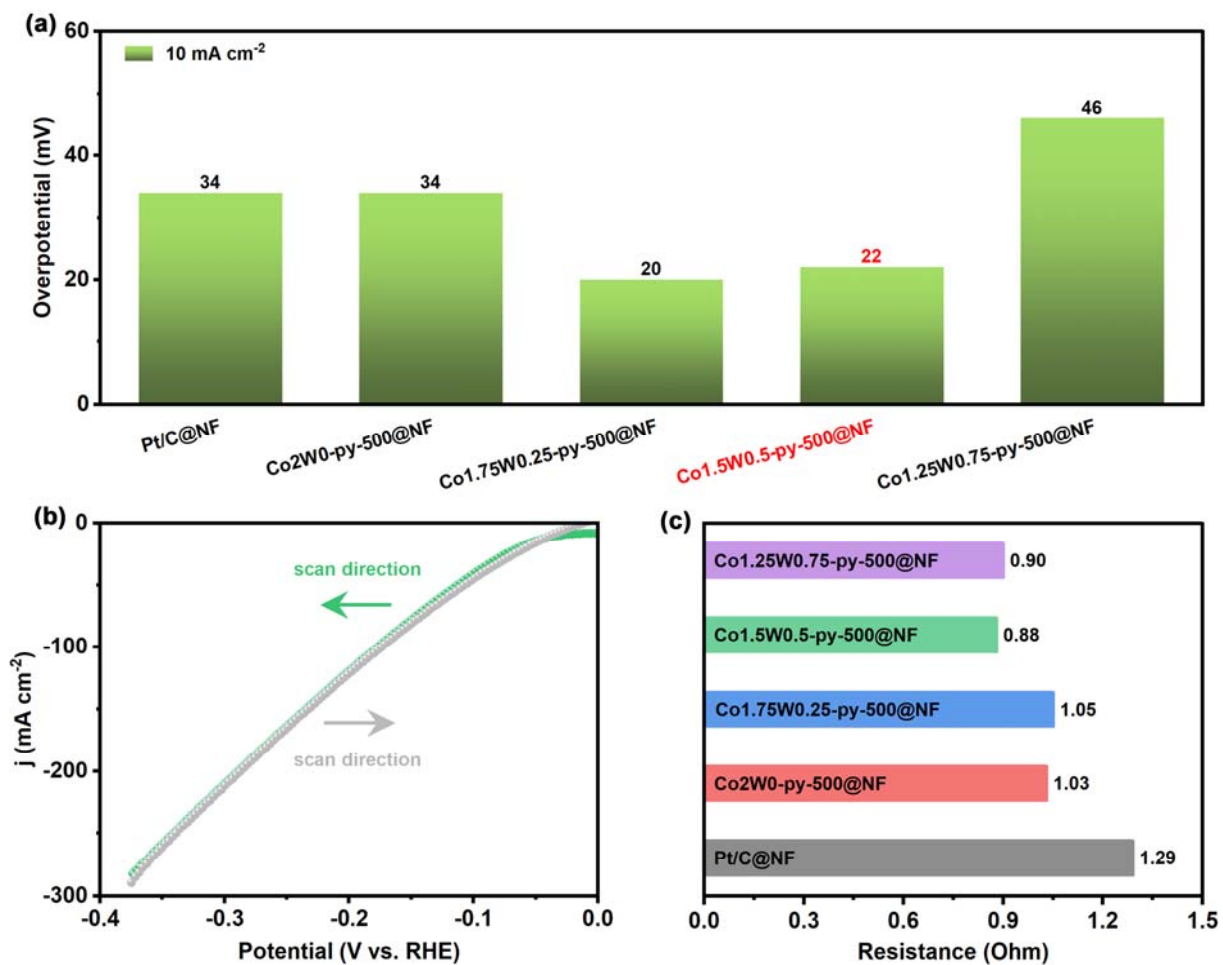
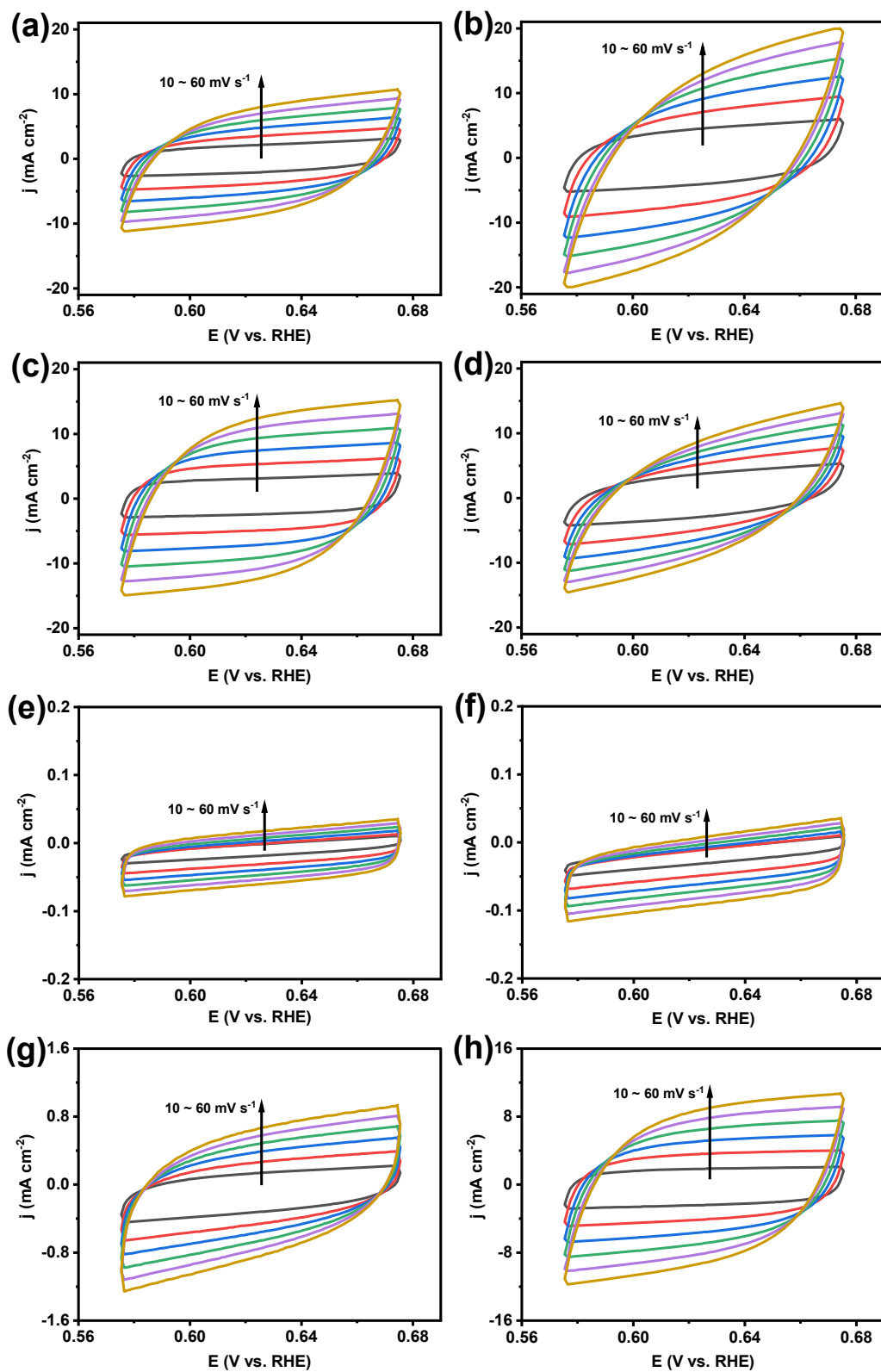


Fig. S10. Raman spectra of Co<sub>1.5</sub>W<sub>0.5</sub>-py-400, Co<sub>1.5</sub>W<sub>0.5</sub>-py-500 and Co<sub>1.5</sub>W<sub>0.5</sub>-py-600.



**Fig. S11.** (a) Overpotentials at the current density of 10 mA cm<sup>-2</sup>. (b) LSV curves of Co1.5W0.5-py-500@NF obtained from two different scan directions (without iR compensation). (c) R<sub>ct</sub> values of Co2W0-py-500@NF, Co1.75W0.25-py-500@NF, Co1.5W0.5-py-500@NF, Co1.25W0.75-py-500@NF, and Pt/C@NF.



**Fig. S12.** Cyclic voltammograms of (a) Co<sub>2</sub>W<sub>0</sub>-py-500@NF, (b) Co<sub>1.75</sub>W<sub>0.25</sub>-py-500@NF, (c) Co<sub>1.5</sub>W<sub>0.5</sub>-py-500@NF, (d) Co<sub>1.25</sub>W<sub>0.75</sub>-py-500@NF, (e) Co<sub>1.5</sub>W<sub>0.5</sub>-hy@NF, (f) Co<sub>1.5</sub>W<sub>0.5</sub>-mof@NF, (g) Co<sub>1.5</sub>W<sub>0.5</sub>-py-400@NF, and (h) Co<sub>1.5</sub>W<sub>0.5</sub>-py-600@NF.

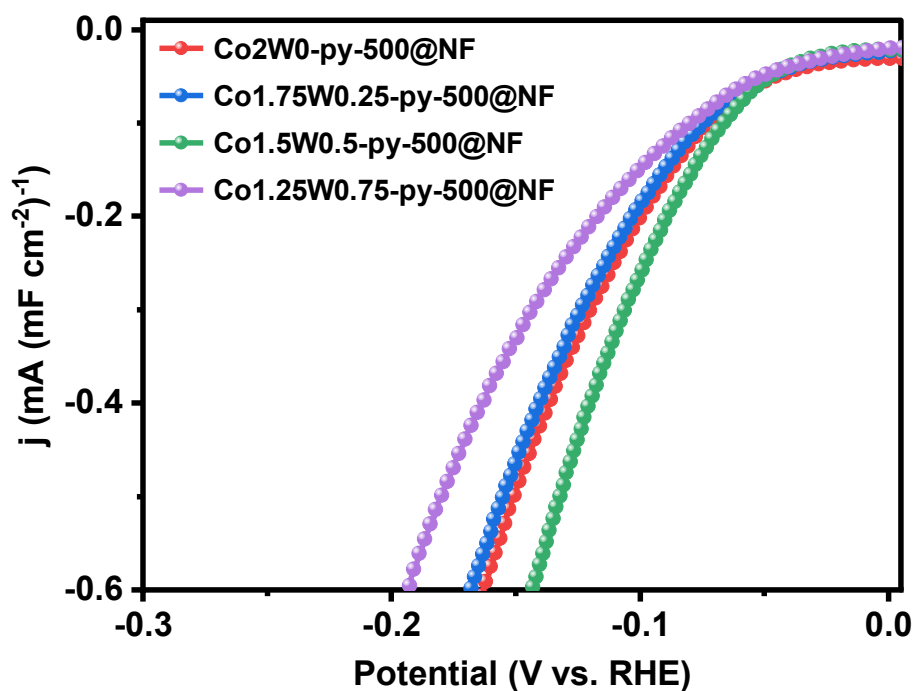


**Fig. S13.**  $C_{\text{at}}$ -normalized LSV curves of Co<sub>2</sub>W<sub>0</sub>-py-500@NF, Co<sub>1.75</sub>W<sub>0.25</sub>-py-500@NF, Co<sub>1.5</sub>W<sub>0.5</sub>-py-500@NF and Co<sub>1.25</sub>W<sub>0.75</sub>-py-500@NF.

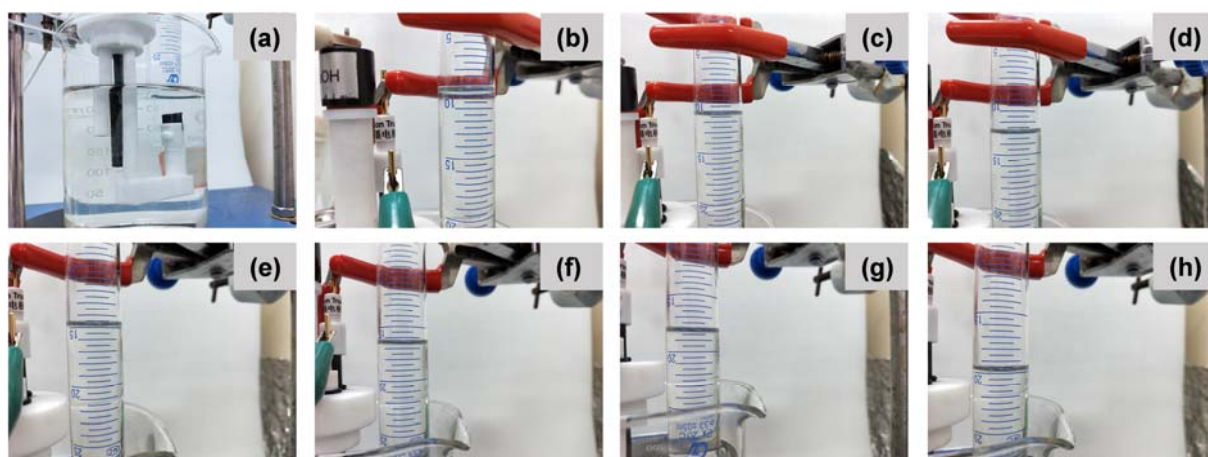


**Fig. S14.** Volume of H<sub>2</sub> collected by drainage method. (a) Device of the drainage method. (b ~ h) Photos taken at (b) 0 min, (c) 10 min, (d) 20 min, (e) 30 min, (f) 40 min, (g) 50 min and (h) 60 min.

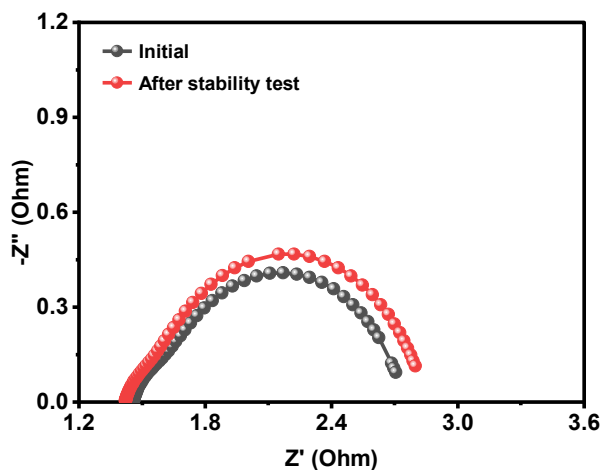


**Fig. S15.** EIS spectra of Co<sub>1.5</sub>W<sub>0.5</sub>-py-500@NF before and after stability test.

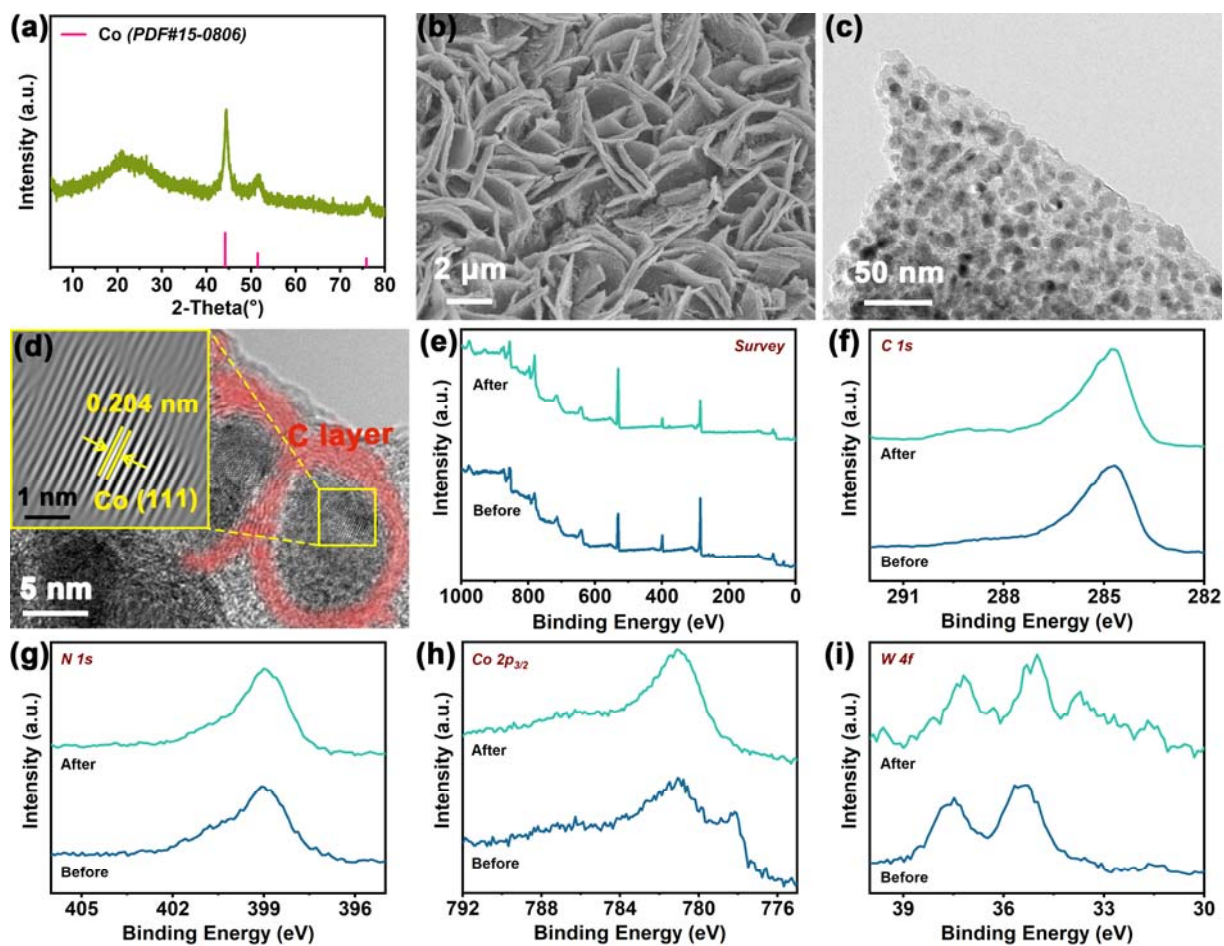


**Fig. S16.** (a) XRD pattern, (b) SEM image, (c) TEM image, (d) HRTEM image of Co<sub>1.5</sub>W<sub>0.5</sub>-py-500 after stability test. (e) Survey, (f) C 1s, (g) N 1s, (h) Co 2p<sub>3/2</sub>, and (i) W 4f XPS spectra of Co<sub>1.5</sub>W<sub>0.5</sub>-py-500@NF before and after stability test.

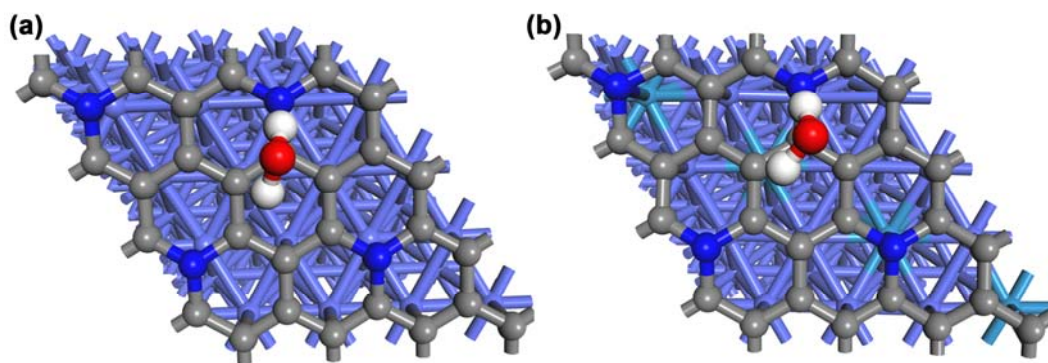


**Fig. S17.** (a) Co@N-C and (b) CoW@N-C structural models, each model has one H<sub>2</sub>O molecule adsorbed at the same active site.

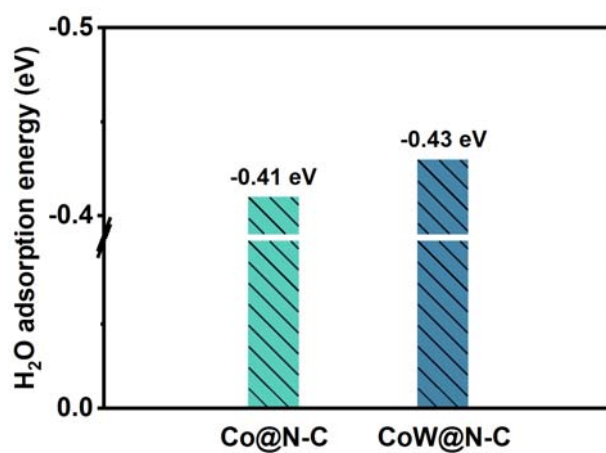


**Fig. S18.** The calculated free energies of water adsorption on Co@N-C and CoW@N-C.

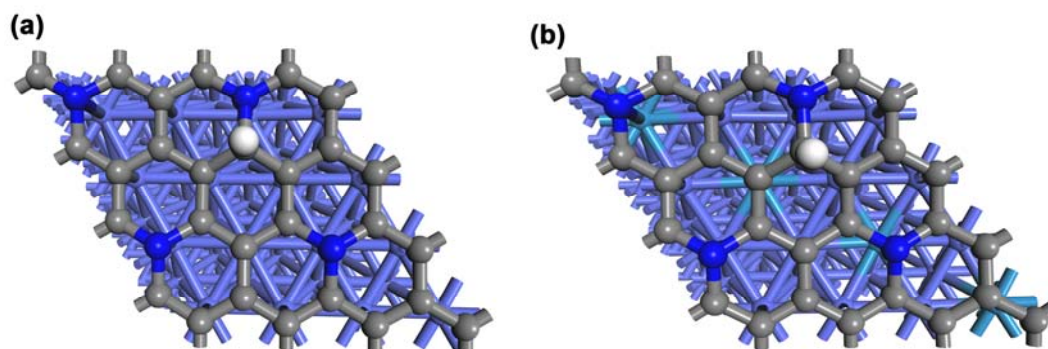


**Fig. S19.** (a) Co@N-C and (b) CoW@N-C structural models, each model has one H intermediate adsorbed at the same active site.

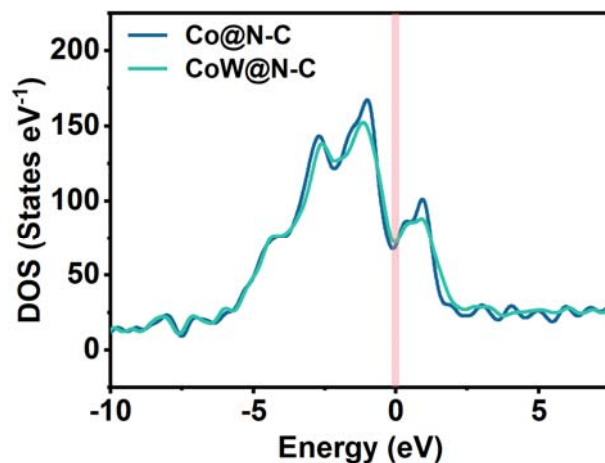


**Fig. S20.** Total electronic density of states (TDOS) of Co@N-C and CoW@N-C. The Fermi level is shifted to zero.

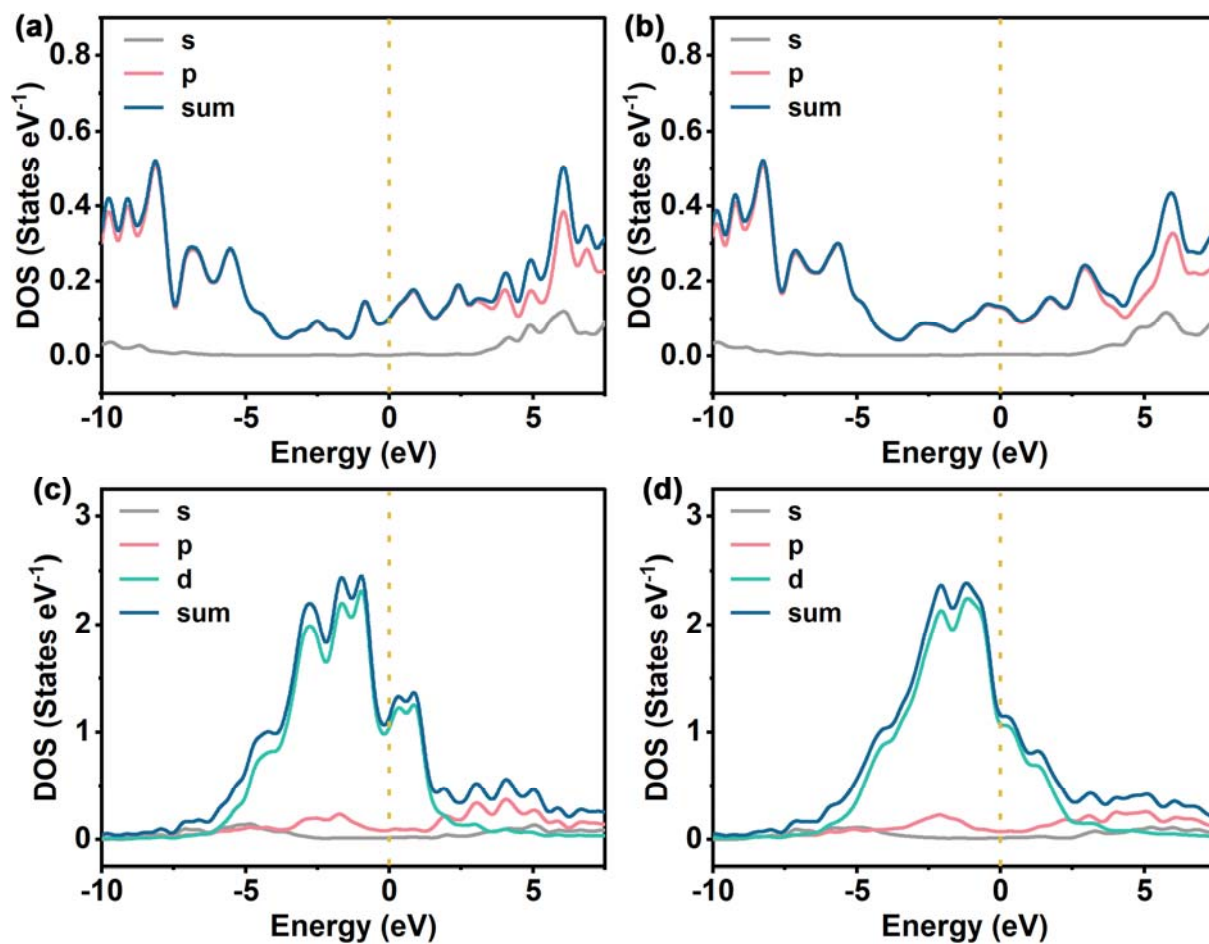


**Fig. S21.** DOS of C atoms in (a) Co@N-C and (b) CoW@N-C projected at different atomic orbitals. DOS of Co atoms in (c) Co@N-C and (d) CoW@N-C projected at different atomic orbitals. The Fermi level is shifted to zero.

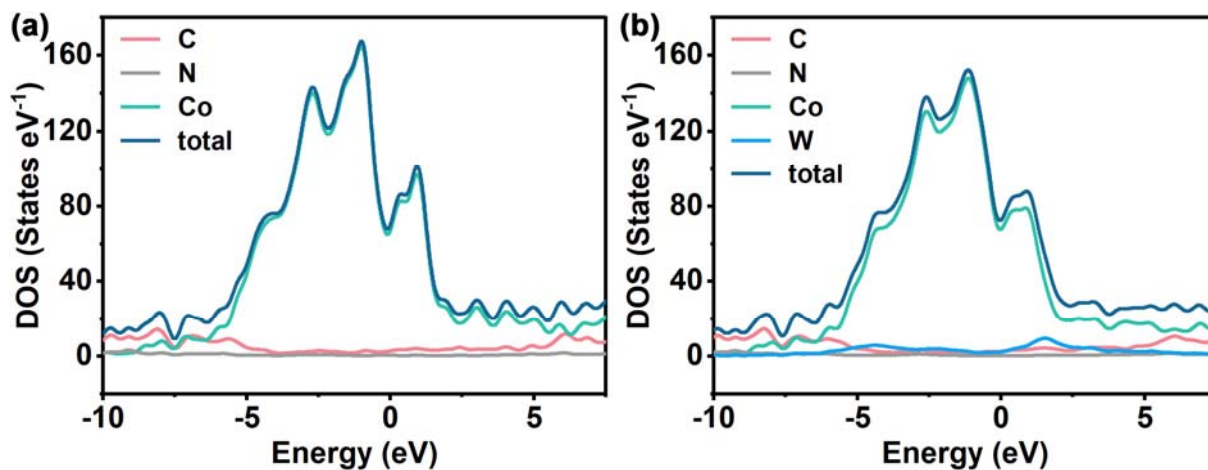


**Fig. S22.** DOS of (a) Co@-NC and (b) CoW@N-C, showing the local DOS from C, N, Co and W atoms. The Fermi level is shifted to zero.

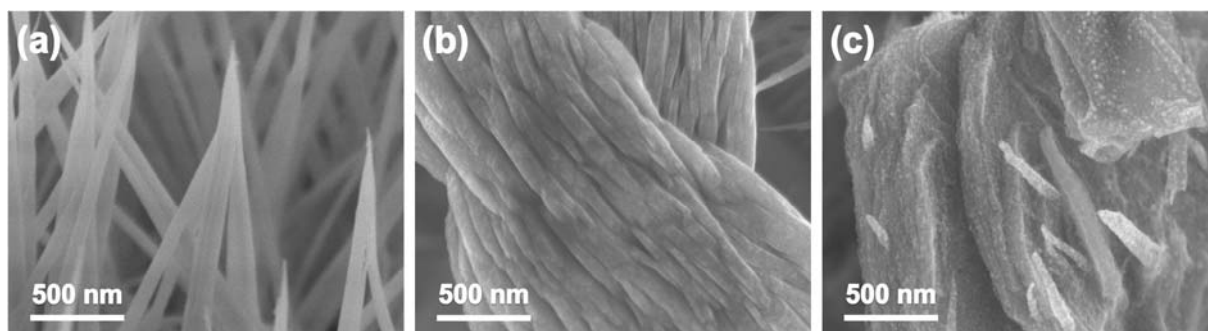


**Fig. S23.** SEM images of (a) CoCr-hy@NF, (b) CoCr-mof@NF and (c) CoCr@N-C@NF.

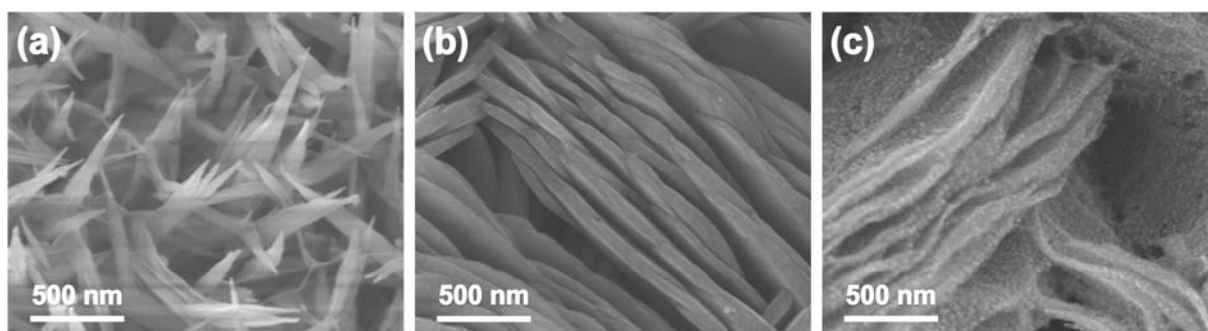


**Fig. S24.** SEM images of (a) CoMo-hy@NF, (b) CoMo-mof@NF and (c) CoMo@N-C@NF.

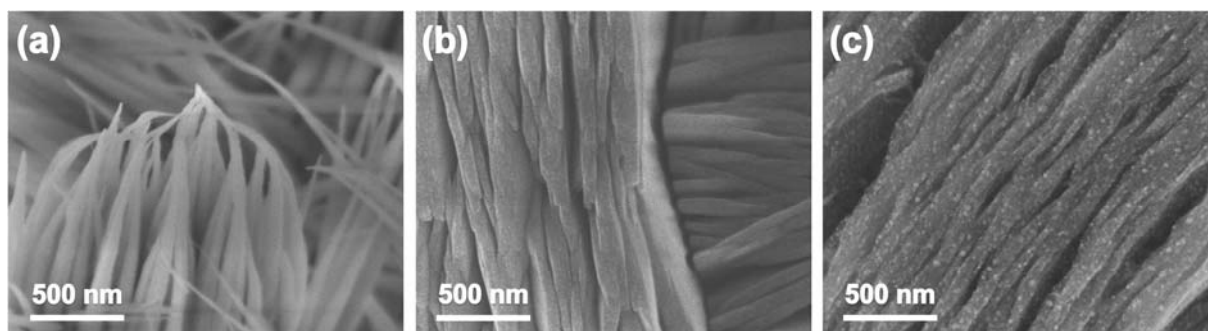


**Fig. S25.** SEM images of (a) CoCe-hy@NF, (b) CoCe-mof@NF and (c) CoCe@N-C@NF.

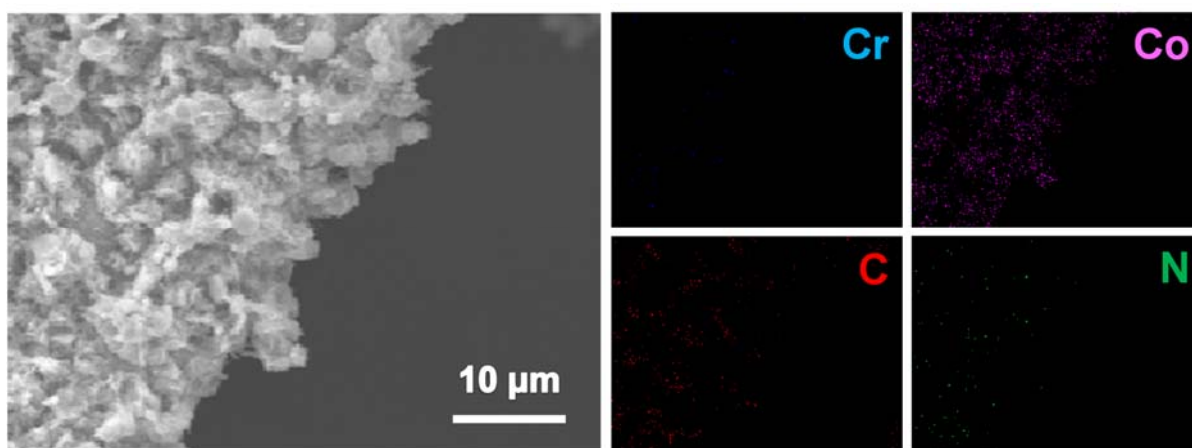


**Fig. S26.** SEM image of CoCr@N-C@NF and the corresponding EDX mapping images of Cr, Co, C and N.

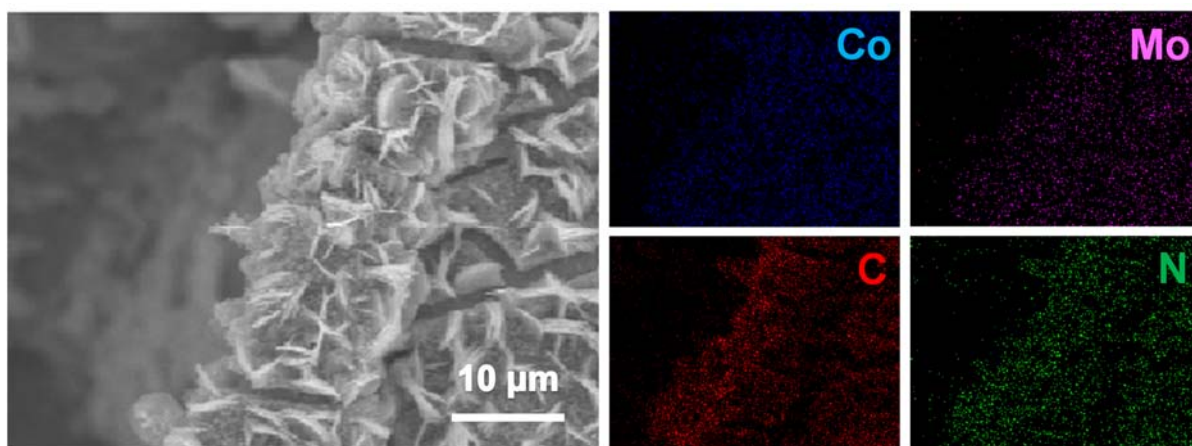


**Fig. S27.** SEM image of CoMo@N-C@NF and the corresponding EDX mapping images of Co, Mo, C and N.

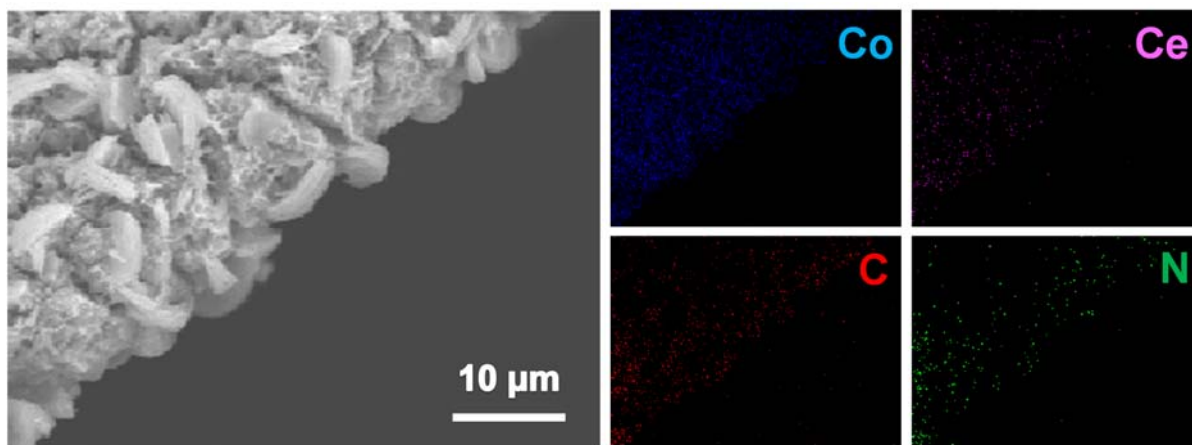


**Fig. S28.** SEM image of CoCe@N-C@NF and the corresponding EDX mapping images of Co, Ce, C and N.

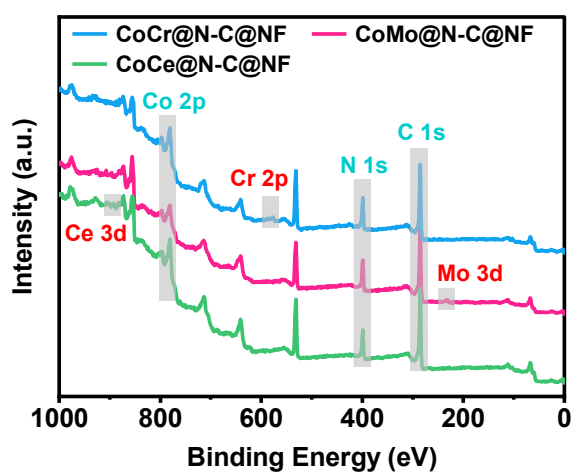


**Fig. S29.** XPS survey spectra of CoCr@N-C@NF, CoMo@N-C@NF and CoCe@N-C@NF.

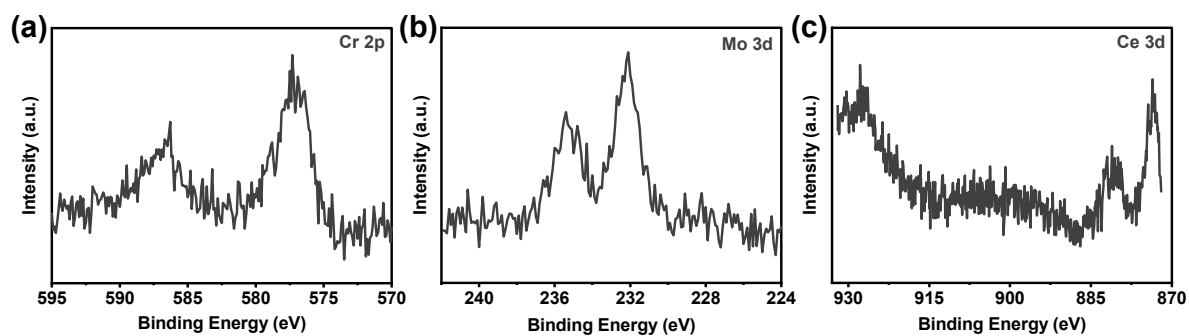


**Fig. S30.** High-resolution XPS spectra of (a) Cr 2p for CoCr@N-C@NF, (b) Mo 3d for CoMo@N-C@NF, and (c) Ce 3d for CoCe@N-C@NF.

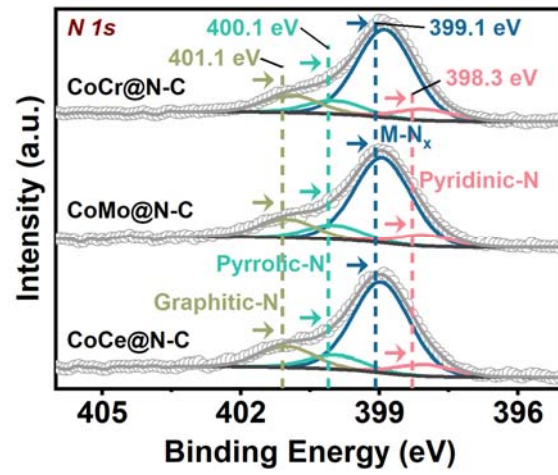


**Fig. S31.** High-resolution XPS spectra of N 1s for CoCr@N-C, CoMo@N-C, and CoCe@N-C.

**Table S1.** Comparison of the electrocatalytic activities of Co<sub>1.5</sub>W<sub>0.5</sub>-py-500@NF with recently reported Co-carbon-based catalysts for HER in 1.0 M KOH.

| Material                                      | Substrate               | Current density<br>(mA cm <sup>-2</sup> ) | Overpotential<br>(mV) | Tafel slope<br>(mV dec <sup>-1</sup> ) | Ref.      |
|---|-------------------------|---|-----------------------|--|-----------|
| Co <sub>1.5</sub> W <sub>0.5</sub> -py-500@NF | Nickel foam             | 10  | 22                    | 63.9                                   | This work |
|   |                         | 25  | 55                    |  |           |
|   |                         | 100                                       | 100                   |  |           |
| Co-NC-750°C                                   | Carbon cloth            | 10  | 73                    | 77                                     | 10        |
| CoP <sub>x</sub> @CNS                         | Nickel foam             | 10  | 91                    | 129                                    | 11        |
| Co <sub>6</sub> W <sub>6</sub> C@NC/CC        | Carbon cloth            | 10  | 59                    | 45.39                                  | 12        |
|   |                         | 50  | 110                   |  |           |
| CoP-InNC@CNT                                  | Glassy carbon electrode | 10  | 159                   | 56                                     | 13        |
| Co-NC/CF                                      | Carbon fiber            | 10  | 157                   | 109                                    | 5         |
| Cu-Foam@CuCoNC-500                            | Copper foam             | 10  | 59.2                  | 81.5                                   | 14        |
| CoP/Co-MOF                                    | Carbon fiber            | 10  | 34                    | 56                                     | 15        |
| Co@N-CS/N-HCP@CC                              | Carbon cloth            | 10  | 66                    | 65                                     | 16        |
| Co <sub>3</sub> S <sub>4</sub> /EC-MOF        | Carbon cloth            | 10  | 84                    | 82                                     | 17        |
|   |                         | 100                                       | 183                   |  |           |
| S-CoWP@(S, N)-C                               | Carbon cloth            | 10  | 67                    | 66                                     | 18        |
| PMo/ZIF-67-6-6N                               | Glassy carbon electrode | 10  | 83                    | 50                                     | 19        |
|   |                         | 100                                       | 202                   |  |           |
| Co@N-CNTs@rGO                                 | Glassy carbon electrode | 10  | 108                   | 55                                     | 20        |
| CoP/NCNHP                                     | Glassy carbon electrode | 10  | 115                   | 66                                     | 21        |
| Ni@CoO@CoNC                                   | Nickel foam             | 10  | 190                   | 98                                     | 22        |

**Table S2.** The values of  $R_s$  calculated based on the EIS spectra of various catalysts in our work.

| <b>Samples</b>                                  | <b><math>R_s</math> (Ohm)</b> |
|---|-------------------------------|
| Pt/C@NF   | 1.62                          |
| Co <sub>2</sub> W <sub>0</sub> -py-500@NF       | 1.64                          |
| Co <sub>1.75</sub> W <sub>0.25</sub> -py-500@NF | 1.61                          |
| Co <sub>1.5</sub> W <sub>0.5</sub> -py-500@NF   | 1.54                          |
| Co <sub>1.25</sub> W <sub>0.75</sub> -py-500@NF | 1.57                          |
| Co <sub>1.5</sub> W <sub>0.5</sub> -hy-@NF      | 1.59                          |
| Co <sub>1.5</sub> W <sub>0.5</sub> -mof-@NF     | 1.53                          |
| Co <sub>1.5</sub> W <sub>0.5</sub> -py-400-@NF  | 1.60                          |
| Co <sub>1.5</sub> W <sub>0.5</sub> -py-600-@NF  | 1.84                          |

## References

- 1 J. Lv, P. Liu, R. Li, L. Wang, K. Zhang, P. Zhou, X. Huang and G. Wang, *Appl. Catal. B-Environ.*, 2021, **298**, 120587.
- 2 M. D. Segall, P. J. D. Lindan, M. J. Probert, C. J. Pickard, P. J. Hasnip, S. J. Clark and M. C. Payne, *J. Phys.: Condens. Matter*, 2002, **14**, 2717-2744.
- 3 J. P. Perdew, M. Ernzerhof and K. Burke, *J. Chem. Phys.*, 1996, **105**, 9982-9985.
- 4 Z. W. Seh, J. Kibsgaard, C. F. Dickens, I. Chorkendorff, J. K. Norskov and T. F. Jaramillo, *Science*, 2017, **355**, eaad4998.
- 5 H. Huang, S. Zhou, C. Yu, H. Huang, J. Zhao, L. Dai and J. Qiu, *Energy Environ. Sci.*, 2020, **13**, 545-553.
- 6 A. Tkatchenko and M. Scheffler, *Phys. Rev. Lett.*, 2009, **102**, 073005.
- 7 J. K. Nørskov, T. Bligaard, A. Logadottir, J. R. Kitchin, J. G. Chen, S. Pandelov and U. Stimming, *J. Electrochem. Soc.*, 2005, **152**, J23-J26.
- 8 B. Liu, Y. F. Zhao, H. Q. Peng, Z. Y. Zhang, C. K. Sit, M. F. Yuen, T. R. Zhang, C. S. Lee and W. J. Zhang, *Adv. Mater.*, 2017, **29**, 1606521.
- 9 Y. Zheng, Y. Jiao, Y. Zhu, L. H. Li, Y. Han, Y. Chen, A. Du, M. Jaroniec and S. Z. Qiao, *Nat. Commun.*, 2014, **5**, 3783.
- 10 Y. T. Zhong, Y. T. Lu, Z. H. Pan, J. Yang, G. H. Du, J. W. Chen, Q. K. Zhang, H. B. Zhou, J. Wang, C. S. Wang and W. S. Li, *Adv. Funct. Mater.*, 2021, **31**, 2009853.
- 11 C. C. Hou, L. Zou, Y. Wang and Q. Xu, *Angew. Chem. Int. Ed.*, 2020, **59**, 21360-21366.
- 12 J. Chen, B. Ren, H. Cui and C. Wang, *Small*, 2020, **16**, 1907556.
- 13 L. Chai, Z. Hu, X. Wang, Y. Xu, L. Zhang, T. T. Li, Y. Hu, J. Qian and S. Huang, *Adv.*

- Sci.*, 2020, **7**, 1903195.
- 14 H. Sun, Q. Li, Y. Lian, C. Zhang, P. Qi, Q. Mu, H. Jin, B. Zhang, M. Chen, Z. Deng and Y. Peng, *Appl. Catal. B-Environ.*, 2020, **263**, 118139.
  - 15 T. Liu, P. Li, N. Yao, G. Cheng, S. Chen, W. Luo and Y. Yin, *Angew. Chem. Int. Ed.*, 2019, **58**, 4679-4684.
  - 16 Z. Chen, Y. Ha, H. Jia, X. Yan, M. Chen, M. Liu and R. Wu, *Adv. Energy Mater.*, 2019, **9**, 1803918.
  - 17 T. Liu, P. Li, N. Yao, T. Kong, G. Cheng, S. Chen and W. Luo, *Adv. Mater.*, 2019, **31**, 1806672.
  - 18 B. Weng, C. R. Grice, W. Meng, L. Guan, F. Xu, Y. Yu, C. Wang, D. Zhao and Y. Yan, *ACS Energy Lett.*, 2018, **3**, 1434-1442.
  - 19 C. Chen, A. Wu, H. Yan, Y. Xiao, C. Tian and H. Fu, *Chem. Sci.*, 2018, **9**, 4746-4755.
  - 20 Z. Chen, R. Wu, Y. Liu, Y. Ha, Y. Guo, D. Sun, M. Liu and F. Fang, *Adv. Mater.*, 2018, **30**, 1802011.
  - 21 Y. Pan, K. Sun, S. Liu, X. Cao, K. Wu, W. C. Cheong, Z. Chen, Y. Wang, Y. Li, Y. Liu, D. Wang, Q. Peng, C. Chen and Y. Li, *J. Am. Chem. Soc.*, 2018, **140**, 2610-2618.
  - 22 G. Cai, W. Zhang, L. Jiao, S. H. Yu and H. L. Jiang, *Chem*, 2017, **2**, 791-802.